Minimum metallic conductivity of fluid hydrogen at 140 GPa (1.4 Mbar)

W. J. Nellis, S. T. Weir, and A. C. Mitchell
Lawrence Livermore National Laboratory, University of California, Livermore, California 94550
(Received 16 June 1997; revised manuscript received 12 October 1998)

Electrical conductivity measurements indicate that fluid hydrogen achieves the minimum conductivity of a metal at 140 GPa, ninefold initial liquid-H_2 density, and 2600 K. Metallization density is defined to be that at which the electronic mobility gap E_g is reduced by pressure to $E_g \sim k_B T$, at which point E_g is filled in by fluid disorder to produce a metallic density of states with a Fermi surface and the minimum conductivity of a metal. High pressures and temperatures were obtained with a two-stage gun, which accelerates an impactor up to 7 km/sec. A strong shock wave is generated on impact with a holder containing liquid hydrogen at 20 K. The impact shock is split into a shock wave reverberating in hydrogen between two stiff Al_2O_3 anvils. This compression heats hydrogen quasi-isentropically to about twice its melting temperature and lasts ~100 ns, sufficiently long to achieve equilibrium and sufficiently short to preclude loss of hydrogen by diffusion and chemical reactions. The measured conductivity increases four orders of magnitude in the range 93 to 140 GPa and is constant at 2000 $(\Omega\,\mathrm{cm})^{-1}$ from 140 to 180 GPa. This conductivity is that of fluid Cs and Rb undergoing the same transition at 2000 K. This measured value is within a factor of 5 or less of hydrogen conductivities calculated with (i) minimum conductivity of a metal, (ii) Ziman model of a liquid metal, and (iii) tight-binding molecular dynamics. At metallization this fluid is ~90 at. % H_2 and 10 at. % H with a Fermi energy of ~12 eV. Fluid hydrogen at finite temperature undergoes a Mott transition at $D_m^{1/3} a^* = 0.30$, where D_m is the metallization density and a^* is the Bohr radius of the molecule. Metallization occurs at a lower pressure in the fluid than predicted for the solid probably because crystalline and orientational phase transitions in the ordered solid do not occur in the fluid and because of many-body and structural effects. Tight-binding molecular dynamics calculations by Lenosky *et al.* suggest that fluid metallic hydrogen is a novel state of condensed matter. Protons are paired transiently and exchange on a timescale of a few molecular vibrational periods, $\sim 10^{-14}$ sec. Also, the kinetic, vibrational, and rotational energies of the dynamically paired protons are comparable. [S0163-1829(99)02805-2]

I. INTRODUCTION

Determining properties of hydrogen ($Z=1$) at very high pressures is challenging experimentally because of the difficulty in achieving extreme conditions and challenging theoretically because of the large zero-point motions of the molecule and absence of core electrons in the atom. As a result, standard theoretical approximations are not valid for hydrogen and experiments are essential.

Solid hydrogen has been the prototypical system of the insulator-to-metal (IM) transition ever since Wigner and Huntington predicted that the insulating molecular solid would transform to a conducting monatomic solid at sufficiently high pressure P and density D at temperature $T = 0$ K.[1] Substantial pressure is required to do this because solid molecular hydrogen is a wide bandgap insulator at ambient ($E_g = 15$ eV). Since Wigner and Huntington, the predicted pressure of this transition has varied from 25 (Ref. 1) to 2,000 GPa (Ref. 2) at 0 K. Raman vibron data[3] suggest metallization might occur at 300 GPa.[4] Calculations of this IM transition with an intermolecular potential derived from shock data and theory of the monatomic metal predict an IM transition at 300–400 GPa.[5] Metallization might occur within the molecular solid phase itself. Electronic bandgaps calculated for diatomic hydrogen at 0 K predict metallization pressures in the range 150–300 GPa, depending on molecular orientation in the hcp phase.[6,7] However, the hcp structure is energetically unfavorable and lower energy structures have wider band gaps.[8] Thus, the transition pressure is structure dependent and the crystal structure at metallization at 0 K is not known.

Experimentally, solid hydrogen at 300 K is transparent at pressures up to 340 GPa, indicative of the insulating state.[9] Pressure-volume data have been measured by x-ray diffraction in the hcp solid up to 120 GPa.[10] These data suggest the dissociative transition pressure in the solid might be as large as 620 GPa. The metallic solid has not been observed in optical spectroscopy experiments in the range 190 to 290 GPa.[11–13]

In the fluid, electrical conductivity measurements under shock compression indicate that hydrogen becomes metallic at 140 GPa, ninefold initial liquid density, and ~3000 K.[14,15] Metallization occurs under pressure when the electronic band gap decreases from 15 eV at ambient[16] down to ~0.25 eV (3000 K), the temperature. Extrapolation of the melting curve of H_2 measured at relatively low pressures[17,18] gives a melting temperature of ~1500 K at 140 GPa, which is comparable to theoretical predictions.[19,20] Thus, this observed metallization most probably occurs within the warm fluid. Metallization in the cold solid, as predicted by Wigner and Huntington, is yet to be observed.

Electrical conductivity has also been measured under single-shock compressions up to 20 GPa and 4600 K.[21] Those measurements show that electronic conduction is thermally activated in the semiconducting fluid. Electrical conductivity experiments using explosively driven magnetic flux

 ©1999 The American Physical Society

compression to isentropically compress liquid hydrogen have shown that the conductivity becomes greater than 1 $(\Omega\,\mathrm{cm})^{-1}$ at 200 GPa and 400 K.[22] Although that conductivity is not metallic, that experiment demonstrates that electrical conductivity increases at high pressure and temperature. Shock Hugoniot (pressure-volume) and temperature data have also been measured for fluid deuterium and hydrogen.[23–28]

Hydrogen is of great importance for planetary science because its cosmological abundance is about 90 at. %. Jupiter and Saturn contain over 400 Earth masses, most of which is hydrogen. The interiors of giant planets are at high pressures and high temperatures in the fluid[19,20] because of their large mass and low thermal conductivity. Implications for Jupiter of our recent measurements on hydrogen have been discussed.[29–33]

The equation of state of fluid hydrogen is important for inertial confinement fusion (ICF). In laser-driven ICF a fuel pellet composed of the hydrogen isotopes deuterium and tritium is placed in a hohlraum and radiated by a multistepped, high-intensity laser pulse.[34,35] The first step of the laser pulse produces a ~100 GPa shock and the successive pulses comprise a quasi-isentrope, similar to the compressive process used in these conductivity experiments. In order to achieve efficient nuclear-fusion reaction of deuterium and tritium, it is necessary to achieve the highest possible areal mass density of the deuterium-tritium fuel. In order to achieve a relatively high areal mass density with a relatively low investment of laser energy, it is necessary to compress most of the deuterium-tritium fuel on a low-lying isentrope. This is accomplished by achieving maximum first-shock density with the lowest possible entropy. These electrical conductivity measurements yield electronic excitation energies which are needed to calculate the equation of state of hydrogen in this regime of importance to ICF. Scientific and technological possibilities for metastable solid metallic hydrogen if it could be quenched to ambient, including room-temperature superconductivity,[36,37] are discussed elsewhere.[38]

Because of the high kinetic energy (0.5 MJ) of the impactor which produces high pressures in these experiments, we are working at a confluence of high-energy and condensed matter physics. This energy is comparable to the total kinetic energy of the proton-antiproton beams in the Tevetron at the Fermi National Accelerator Laboratory.[39] This kinetic energy enables discovery of novel states of condensed matter, analogous to the discovery of novel states of subnuclear matter. The purpose of this paper is to describe details of the shock compression experiments which were used to measure electrical conductivities of dense fluid hydrogen as it undergoes the transition from a semiconductor to a state with the minimum conductivity of a metal.

II. FINITE TEMPERATURES

The distinguishing feature of these experiments is the achievement of hydrogen at 3000 K (0.3 eV) and 100 GPa pressures. A temperature of 0.3 eV is relatively low and the fluid is quantum in nature because the Fermi energy is ~12 eV, which means the electronic system is degenerate, and because the spacing between the first few vibrational levels of the H_2 molecule is ~6000 K,[40] which means the system is essentially a quantum-mechanical harmonic oscillator with a zero-point vibrational energy of ~3000 K. This quantum metallic fluid is primarily molecular with some of the molecules in an excited vibrational state and ~10 at. % H. Virtually all previous high-pressure hydrogen experiments have been performed on a crystalline solid at room temperature or below. Possible explanations for this include (i) theoretical predictions of metallization have all been based on calculations at 0 K. (ii) It is extremely difficult to statically heat hydrogen in a diamond anvil cell because static heating of hydrogen often causes diamond anvils to fail[17,18] and the diffusion coefficient of hydrogen at high temperatures is sufficiently large that the hydrogen sample rapidly diffuses away into the diamonds and gasket which contain the hydrogen.[18] For this reason hydrogen experiments are often performed in diamond anvil cells cooled to 77 K.[41] (iii) In general, disorder is expected to delay the onset pressure of metallization from band overlap.[42] For example, molecular-H_2 orientational disorder on an hcp lattice at $T=0$ K requires twice the metallization pressure than if the molecular axis is aligned.[7] This result suggested that disorder in general inhibits metallization, which is not true in the case of hydrogen.

Given that hydrogen metallization has not been observed at high static pressures, it is desirable to find a way to lower the metallization pressure so it can be observed. The pressure required for the IM transition in a solid, or more properly the nonmetal-metal (NMM) transition at finite temperature, is known to decrease with temperature.[43] In addition, phenomena which inhibit metallization in dense solid H_2; namely, crystalline and orientational phase transitions,[44,45] do not occur in a disordered fluid. Thus, it is desirable to look for the NMM transition at higher temperatures in the fluid. Shock compression is ideal because the sample is heated instantaneously, adiabatically, and uniformly on compression and the temporal width of a shock front is <1 ps. It is also essential to use a temperature pulse. The duration of the pulse should be sufficiently long to achieve equilibrium and sufficiently short that the hydrogen sample cannot diffuse away nor react chemically. The ~100 ns duration of shock compression satisfies these criteria.

III. EXPERIMENT

A layer of liquid H_2 or D_2 at 20 K is compressed by a high-pressure shock wave reverberating between two stiff, electrically insulating anvils. The compression is initiated by a strong impact-generated shock incident from one of the anvils into the liquid hydrogen. Electrical resistance of the hydrogen sample is measured versus time by inserting electrodes through the other anvil, as illustrated in Fig. 1.

The incident shock was produced by impact of a planar metal plate accelerated up to ~7 km/sec with a two-stage light-gas gun. A two-stage gun, illustrated in Fig. 2, achieves higher velocities and twice the shock pressures achieved with a plane-wave explosive system and is a reusable laboratory facility. Each stage consists of driving gas plus projectile, either a piston or an impactor. This gun consists of a breech containing up to 3.5 kg of gunpowder and a pump tube filled with 60 g of hydrogen gas, not to be confused with the liquid-hydrogen target. The rupture valve consists of two steel disks each with two perpendicular groves chosen

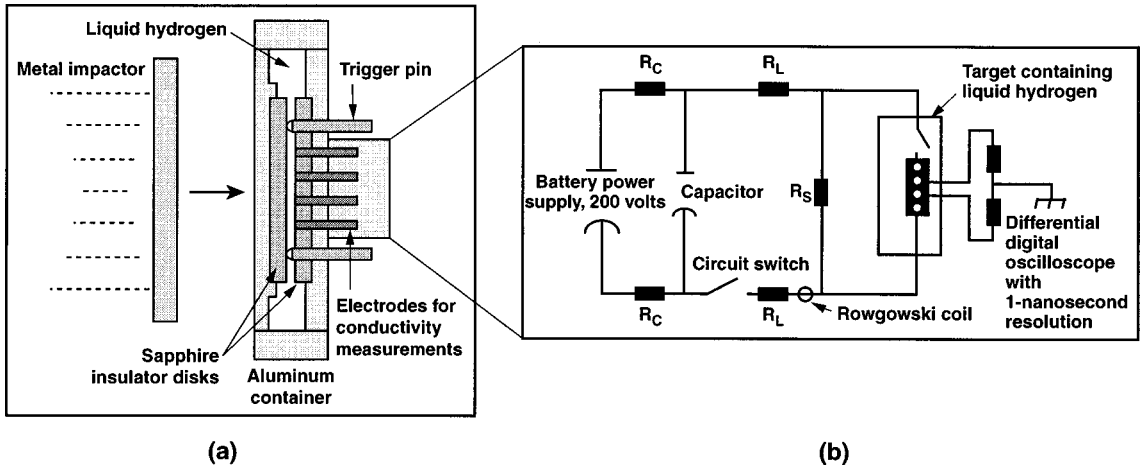

FIG. 1. Schematic of electrical conductivity experiments (not to scale). Four electrodes in (a) were connected to circuit in (b). For conductivities lower than metallic, two probes were used. Metal impactor is accelerated to ~7 km/sec with gas gun in Fig. 2.

such that this valve opens when the hydrogen gas pressure in the pump tube reaches ~0.1 GPa. The highest impactor velocity is achieved with the driving gas having the highest sound velocity c in order to transmit pressure to the impactor at the most rapid rate. Since the driving gas behaves essentially as an ideal gas, $c=(\gamma k_B T/M)^{0.5}$, where γ is the ratio of specific heat at constant pressure to that at constant volume, k_B is Boltzmann's constant, T is the temperature of the compressed gas, and M is its molecular weight. Since hydrogen has the smallest M of any gas, it has the highest sound velocity and, thus, achieves the highest impactor velocity and pressure of any driving gas.

The 25-mm-diameter impactor plate consisted either of an Al or Cu plate 3.0-mm thick, hot-pressed into a Lexan polycarbonate sabot. Hot gases from the burning gunpowder drive a heavy piston (4.5 to 6.8 kg) down the pump tube, which is 10-m long and 90 mm in diameter, compressing the hydrogen gas. At a pressure of about 0.1 GPa, the gas breaks the rupture valve and enters the narrower, evacuated barrel, 9-m long and 28 mm in diameter, accelerating the 20-g impactor toward the target. The mass flow rate of the driving gas is constant because the weight of the piston is large compared to that of the gas. Thus, the reduction in diameter from pump tube to barrel causes the velocity of the gas to increase substantially. The magnitude of the pressure generated by the impact is determined by the measured impact velocity[46] and the Hugoniot equations of state of impactor and target.[47,48]

In order for the hydrogen sample to achieve the highest densities and lowest temperatures at high pressures, the sample must have a relatively high initial density. High initial densities were achieved by using a liquid sample near the saturation curve at atmospheric pressure and 20 K.[25,49] Since the sample holder is destroyed by the impactor, a new one is required for each experiment.

We have measured electrical conductivities of several liquids[21,50–53] and applied these techniques to the configuration illustrated in Fig. 1. The liquid H_2 or D_2 sample was 0.5-mm thick, 25 mm in diameter, and contained between two electrically insulating sapphire (single-crystal, z-cut Al_2O_3) anvils, 2.0-mm thick and 25 mm in diameter. In turn, these sapphire disks are contained between two 2.0-mm-thick Al (alloy 1100) disks of the main body of the Al cryogenic target assembly. Al is strong, ductile, and a good thermal conductor at 20 K, which facilitates condensing the sample from high-purity gas. The Al_2O_3 disk containing the electrodes and the adjacent Al disk were bonded together by a thin glue layer. The room-temperature densities of the sapphire and Al (alloy 1100) were 3.99 and 2.712 g/cm^3, respectively. The hydrogen layer was relatively thin (0.5 mm) so that the experiment would have a sufficiently short time duration that deleterious effects could not occur (interfacial instabilities and loss of the high-temperature hydrogen by mass diffusion and chemical reactions), while being sufficiently long to achieve thermal and electrical equilibrium.

As discussed below, the strong single shock incident from the stiff Al_2O_3 disc, or anvil, on the leftside of the soft hydrogen [Fig. 1(a)] is split into multiple, relatively weak shocks reverberating in hydrogen between the two Al_2O_3 an-

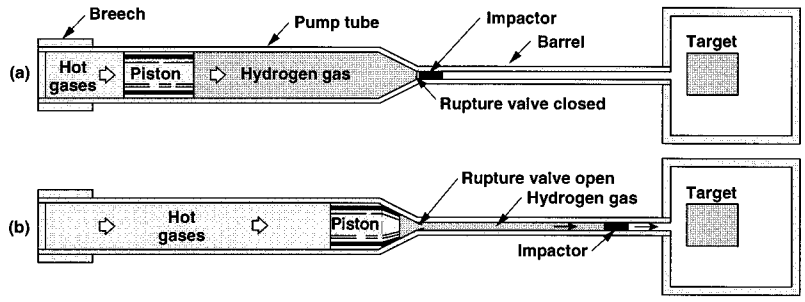

FIG. 2. Schematic of two-stage light-gas gun. Gas gun used in these experiments is 19-m long.

vils. Each time one of these shocks strikes the anvil on the right a portion of the wave is reflected back into the hydrogen, compressing it further, and the other portion is transmitted forward into the Al_2O_3. Each transmitted shock is at successively higher pressure and velocity until the final pressure is reached. At this point the leading shock is again a strong single wave. Because the hydrogen layer is initially only 0.5-mm thick and compresses a factor of ~10, the reverberation is completed well before the leading shock exits the Al_2O_3, which is initially 2.0 mm thick and compresses only a factor of ~1.4. The experiment is over when the leading shock wave exits the Al_2O_3 containing the electrodes. When the leading shock reaches the rear interface between Al and vacuum, the sample holder blows out and is destroyed. Since shock velocities are ~10 km/sec and the voltage signals travel at the speed of light of their coaxial cables, the measurement is made prior to destruction of the sample holder.

Either H_2 or D_2 samples were used, depending on the final density and temperature desired. That is, because the initial mass densities of liquid H_2 and D_2 at 20 K differ by a factor of 2.4, their final shock-compressed densities, temperatures, and conductivities also differ substantially at the same final pressure. At the relatively high densities and temperatures achieved, possible effects of different zero-point vibrational energies for hydrogen and deuterium are negligible. Thus, the two isotopes are used to achieve different thermodynamic states, rather than to look for an isotope effect. A calibrated Pt resistance thermometer [not shown in Fig. 1(a)] is inserted into the sample chamber to indicate when the liquid sample is condensed.

Stainless steel (type 302) electrodes to measure electrical resistance exit the sample holder to the right [Fig. 1(a)]. Steel was chosen because it has a shock impedance and thermal contraction similar to Al_2O_3, which makes steel relatively transparent to the shock wave in Al_2O_3 and less likely to open a vacuum leak at low temperature prior to the experiment. In addition, it has a relatively high electrical resistivity which means that current flow will diffuse relatively rapidly from the outer cylindrical surface in towards the center to produce an equilibrated current density in the 100-ns duration of the experiment. This is important because the calibration calculations relating resistance to resistivity assume that current density is equilibrated over the cross sectional area of the current electrodes. Also, because stainless steel is an impure alloy, its resistivity changes relatively little on shock compression. The electrodes had flat surfaces which were initially flush with the right interface [Fig. 1(a)] between the hydrogen sample and sapphire anvil. In the metallic phase of hydrogen four electrodes were used; two outer electrodes for current and two inner electrodes to measure potential difference. These electrodes were collinear and 0.75 mm in diameter with 1.5 mm between their centers. Two electrodes 1.0 mm in diameter separated by 3.5 mm between their centers were used if the pressures were such that the hydrogen was a poor conductor and contact resistance was negligible. Trigger pins were used to turn on the recording system, Tektronix DSA 602A digital oscilloscopes and 7103 analog oscilloscopes with ~2 ns time resolution, at the appropriate time. In order to measure relatively low potential differences in a noisy environment, the oscilloscopes were used in a differential mode; i.e., voltage was measured on each probe relative to ground and then voltage difference was determined to eliminate common electrical noise on both cables.

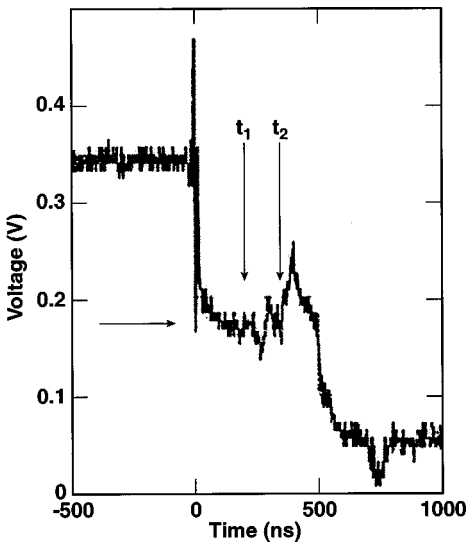

FIG. 3. Voltage versus time measured across two outermost electrodes in experiment at 180 GPa. Initial voltage of 0.34 V is potential difference across shunt resistor R_S [Fig. 1(b)]. When hydrogen conducts under shock compression, resistance of parallel combination of R_S and hydrogen cell decreases relative to R_S. Time is zero at first-shock arrival at electrodes [Fig. 1(a)]; t_1 is time shock exits Al_2O_3; t_2 is time shock reaches rear Al surface of sample holder. Horizontal arrow indicates steady voltage of measured resistance. Experiment is over at t_1.

The electrical circuit for four-probe measurements is shown in Fig. 1(b). All cables are coaxial. A power supply charges a capacitor through two charging resistors R_C (0.5 MΩ). Just prior to impact (~20 μsec) the circuit switch is closed, which causes current to flow in the load resistors R_L (~100 Ω) and in the shunt resistor R_S (0.1 to 5 Ω at 20 K) in parallel with the sample. R_S was a nickel-film resistor whose resistance remains essentially constant when the target cools down from room temperature to 20 K. R_S was ~5 times the resistance of the hydrogen cell and it was mounted on the outside of the cryogenic sample holder. Shock compression switches the hydrogen sample into the circuit when its conductivity becomes significant. The voltages across the two inner probes and across the two outer probes were measured differentially. The voltage across the two outer electrodes (Fig. 3) gives the resistance of the parallel combination of R_S and the hydrogen sample. These voltages were also measured with Tektronix 7103 analog oscilloscopes for redundancy. The current was measured with a Rowgowski coil. Typical currents were ~1 A and voltages were a few tens of mV. The current density in the hydrogen sample was ~500 A/cm^2 for 100 ns.

The voltage measured across the two outermost electrodes, which are in parallel with R_S, is shown versus time in Fig. 3 for the shot at 180 GPa, the maximum pressure in this series. A voltage spike occurs at $t=0$ when the shock first hits the electrodes because of a small tilt ($\sim 1^0$) of the impactor and thus of the shock wave, which causes a slight difference in the shock arrival times at the two electrodes. The voltage then decreases when the hydrogen conductivity

begins to increase and then plateaus after the pressure and the conductivity have reverberated up to their maxima. The shock reverberations are not resolved because of the tilt and the short time duration of each reverberation. The voltage is steady while the shock traverses the insulating Al_2O_3 because the metallic state of hydrogen is equilibrated. This steady voltage gives the electrical resistance of the hydrogen. The experiment is over at t_1, the calculated time at which the shock reaches the interface between the Al_2O_3 and Al. Subsequently, the shock traverses the Al disk and the voltage is erratic because current can flow through the Al if the shock induces conductivity in the thin glue layer holding each electrode in the Al. Eventually the shock reaches the rear Al surface at t_2; this Al surface and the electrodes then blow outward into vacuum toward R_S, causing the signal to change dramatically. The circuit for the two-probe configuration is the same one described previously for measuring the electrical resistivity of sapphire shocked to 100 GPa pressures.[54] For the highest hydrogen resistivities no shunt resistor was used.

The measured electrical resistivity of shock-compressed sapphire is five orders of magnitude larger than that of hydrogen at metallization,[54] which means that sapphire is an electrical insulator in these experiments. The electrically insulating nature of Al_2O_3 at 100 GPa shock pressures is not affected by the fact that Al_2O_3 undergoes a diffusive phase transition at ~100 GPa pressures and ~1000 K.[55] The measured resistivities of Al_2O_3 shocked to 100–200 GPa and ~1000 K (Ref. 54) are much too large to affect these hydrogen conductivity results. Also, electrical conductivities of water were measured in this same sample holder.[56] Water was chosen because its charge carriers and conductivities are expected to be different than those of hydrogen. The dominant charge carrier in water is the proton[57] and its conductivity at these pressures is expected to be similar to that measured previously.[50] As expected, the measured conductivities of water differ from those of hydrogen in terms of their magnitudes and pressure dependance.

Additional issues about the experiment are discussed in the Appendix. Hydrogen conductivities in the semiconducting fluid similar to those reported here have been measured elsewhere using a reverberating shock wave generated with high explosives.[58]

IV. THERMODYNAMIC STATES

A reverberating shock[59–62] achieves states of highly-condensed matter relatively close to the 0 K isotherm. The reverberation for the experiment at 180 GPa is illustrated in Fig. 4(a), plotted as pressure P versus mass velocity u_p because these quantities are continuous across an interface. In Fig. 4(b) the dependence on time t of pressure at the midpoint of the hydrogen layer is shown. The values of the pressure steps are caused by the shock reverberating between the stiff sapphire disks, as illustrated in Fig. 4(a). The values of P, u_p, and t in Fig. 4 were obtained by computational simulation.[63]

Sapphire is extremely strong at shock pressures below 50 GPa, having a Hugoniot elastic limit of ~20 GPa.[64,65] This raises the possibility of a strength-induced two-wave shock structure. However, we measured a single-wave shock in sapphire at 80 GPa, which means that at the 93 GPa and higher in these conductivity experiments the shock waves in Al_2O_3 incident onto the hydrogen sample have a simple single-wave structure.

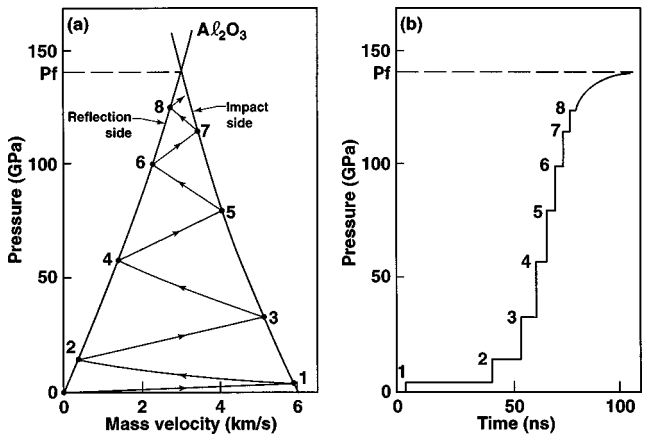

FIG. 4. Shock reverberation in hydrogen. These curves were calculated (Ref. 63) for 140 GPa. (a) Pressure P versus mass velocity u_p. Reflection side is sapphire on right and impact side is sapphire on left in Fig. 1(a). State 1 is first shock in hydrogen; state 2 is reached when first shock reflects off Al_2O_3 on right in Fig. 1(a); etc. Even-numbered (P,u_p) states lie on Al_2O_3 Hugoniot; odd-numbered states lie on mirror reflection of Al_2O_3 Hugoniot. (b) Pressure versus time t at midpoint of hydrogen layer. Time duration of each pressure step shortens as hydrogen compresses. State 1 is shock; states 2 and higher are very weak shocks and comprise a quasi-isentrope. P_f is final pressure in hydrogen, equal to pressure incident from sapphire. Thermal equilibrium is achieved within rise time of each step.

Because sapphire is so stiff, its shock compression and, thus, its shock heating are relatively small. For example, the temperature rise caused by a shock pressure of 100 GPa is only ~1000 K,[66] which causes a very small thermal pressure. As a result, the shock[48] and static[67] P-V curves are nearly identical in the 100 GPa range. Thus, thermal pressure of the Al_2O_3 is negligible and the P-V curve is essentially reversible. Thus, because strength is overdriven and thermal effects are small, the mirror reflection in P-u_p space of the Al_2O_3 Hugoniot is an excellent approximation for pressure release curves of shocks in the 100 GPa pressure range. In Fig. 4(a) the Al_2O_3 curve on the left is its Hugoniot; the Al_2O_3 curve on the right is the pressure release curve, the mirror image of the Hugoniot.

The impact causes an initial pressure P_f in the Al_2O_3. When this shock reaches the liquid hydrogen, the pressure drops until the release pressure of sapphire matches the Hugoniot of liquid hydrogen (state 1 in Fig. 4). This drop is about a factor of 30 in pressure. The shock in hydrogen then reverberates back and forth between the sapphire anvils until the pressure reaches P_f, the pressure incident initially from the sapphire. For a typical initial 5 GPa shock in hydrogen, the pressure increases a factor of 50 000 from ambient, which causes some shock heating. However, the successive reverberations are very weak shocks because the pressure increases only a factor of 4 or less on each of these reflections. Thus, the total of all the shock reflections off sapphire corresponds to a quasi-isentrope. This fast compression process is adiabatic and the hydrogen is heated. About 40% of the final temperature is caused by the first shock and the

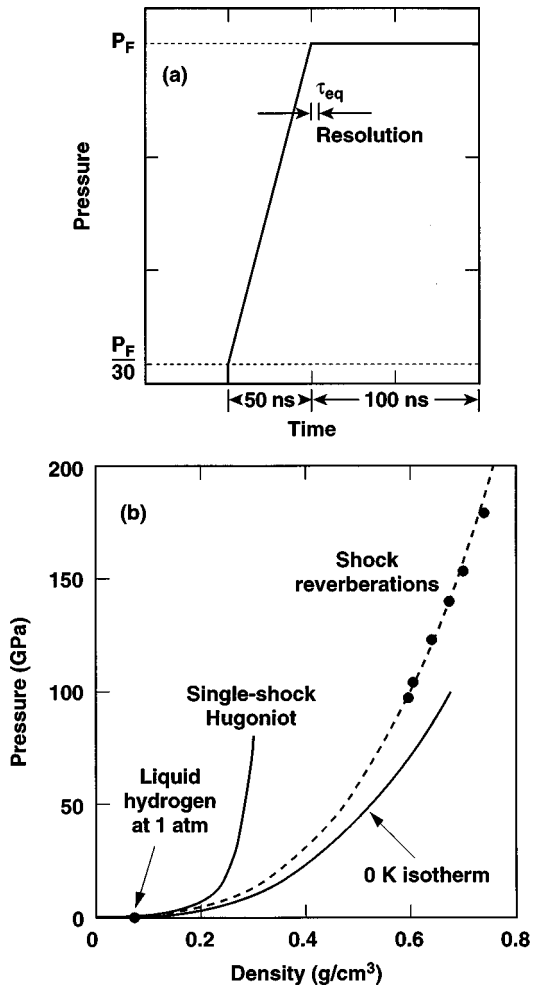

FIG. 5. Illustrations of effect of rise time on pressure. (a) First pressure in hydrogen is $\sim P_f/30$ (state 1 of Fig. 4). Successive reverberations, states 2 and higher in Fig. 4, comprise quasi-isentrope. This quasi-isentrope is represented by ramp over ~50 ns from $P_f/30$ up to P_f. Ramp illustrates that P_f is reached after several 10's ns, which produces isentropic compression, rather than in <ps, which produces shock compression. (b) Equation-of-state curves plotted as pressures versus density: 0 K isotherm, points reached by shock reverberations, and single-shock Hugoniot. Initial point is liquid H_2 at 1 atm and 20 K.

remainder by the quasi-isentrope. This shock reverberation process causes a final temperature which is about an order of magnitude smaller than would be achieved by a single shock to the same final pressure.

The variation of mass velocity of the sapphire with pressure is relatively modest. As maximum pressure increases from 90 to 140 GPa, the mass velocity at P_f increases from 2.16 to 3.03 km/sec. The corresponding mass velocity of state 1 increases from 4.18 to 5.95 km/sec. Electrical resistivity decreases more than three orders of magnitude in this same range.

The pressure pulse applied to hydrogen is illustrated schematically in Fig. 5(a). The initial shock is $P_f/30$. The following quasi-isentrope, which is comprised of the pressure steps in Fig. 4(b), is represented schematically by a ramp in pressure from $P_f/30$ up to P_f. The corresponding effect on the thermodynamics is illustrated in Fig. 5(b). Shock reverberation is necessary to reach metallization near 0.7 g/cm.[3] The various pressure-density curves were calculated using the equation of state of Kerley.[68]

The densities and temperatures must be known to analyze the electrical conductivities. At present there is no way to measure these. Shock temperature is determined by measuring the graybody spectrum of thermal radiation emitted from singly or doubly shocked hydrogen.[26] Although the sapphire anvils are initially transparent, under the series of high-pressure high-rate deformations caused by the shock reverberations, transparent single-crystal sapphire becomes opaque, defected, polycrystalline alumina. Thus, thermal radiation cannot exit the sample and the temperatures must be calculated. The calculational method is the one used previously to calculate pressure history.[25] This calculation also yields density and temperature.

The densities and temperatures were calculated with two representative hydrogen equations of state. The first was developed by Kerley[68] before recent shock data were available and neglects molecular dissociation at the conditions in our experiments. This model is contained in a database for hydrodynamic simulations. Densities and temperatures were calculated by computationally simulating all these impact experiments. As a check on the results, the calculated final pressures in the hydrogen or deuterium all agree to within 1% with the initial shock pressures in the sapphire anvils (P_f in Fig. 4) calculated by shock impedance matching the known Hugoniot equations of state of the impactor and the Al and Al_2O_3 of the sample holder. These results were used in our previous analysis.[15]

The second hydrogen equation of state was that of Ross, which includes molecular dissociation.[26,69,70] This model was not available in a database for hydrodynamic computer simulations. So, hydrogen densities and temperatures were calculated by a method which is different but equivalent to the one above. The first shock pressure in the hydrogen or deuterium was calculated by shock impedance matching the release of the first shock in Al_2O_3 down to the previously measured Hugoniot of hydrogen or deuterium (state 1 in Fig. 4). This shock state was then taken as the initial state of an isentrope, which was calculated up to P_f. Since the first-shock state is different for each experiment, each experiment is on a different isentrope. Since Ross' model is based on experimental data, we take these results as the preferred values, although the basic conclusion is the same for both models. The calculated densities, temperatures, and dissociation fractions are listed in Table I; the pressures were obtained by shock impedance matching.

The results of calculations using both models are plotted in Fig. 6 as density versus pressure and in Fig. 7 as temperature versus pressure. Fig. 6 shows that the densities calculated with the two models differ by about 3%, which is excellent agreement and implies that pressure is relatively insensitive to dissociation. That is, if a molecule dissociates, both of the atoms are still present and contribute to the pressure. The calculated temperatures (Fig. 7) have an offset at 100 GPa. At higher pressures, Ross' model calculates temperatures which increase less rapidly than Kerley's. This is caused by energy absorbed in dissociation which lowers temperature. Based on the differences between these calculations, the systematic uncertainties in calculated density and temperature are 6 and 30%, respectively.

TABLE I. Electrical resistivities of fluid H_2 and D_2. Error bars for resistivities are in parenthesis. Initial densities were 0.071 g/cm^3 for H_2 and 0.171 g/cm^3 for D_2. U_I is impact velocity. Pressures were determined by shock impedance matching Hugoniots of impactor, Al, and sapphire. Densities, temperatures, and dissociation fractions were calculated with model in Ref. 26.

Experiment	Impactor	U_I (km/sec)	Resistivity (Ω cm)	Pressure (GPa)	Density (mol/cm^3)	Temperature (K)	Dissociation fraction
SLDMS4-D_2	Al	5.59	1.4(0.3)	93.1	0.291	2090	7.0×10^{-3}
SLDMS5-D_2	Al	6.76	$1.3(0.5)\times10^{-2}$	121	0.321	2760	4.9×10^{-2}
SLDMS8-D_2	Al	7.33	$2.4(1.2)\times10^{-3}$	135	0.334	3090	9.4×10^{-2}
SLDMS6-H_2	Al	5.90	$3.8(0.8)\times10^{-1}$	100	0.303	1670	2.7×10^{-3}
SLDMS13-H_2	Al	6.10	$1.4(0.5)\times10^{-1}$	105	0.308	1810	5.0×10^{-3}
SLDMS7-H_2	Al	6.90	$7.4(3.0)\times10^{-3}$	124	0.326	2230	2.3×10^{-2}
SLDMS9-H_2	Al	6.91	$3.2(0.7)\times10^{-3}$	124	0.326	2230	2.3×10^{-2}
SLDMS12-H_2	Cu	5.58	$4.2(2.2)\times10^{-4}$	141	0.342	2560	5.7×10^{-2}
SLDMS10-H_2	Cu	5.96	$6.0(1.2)\times10^{-4}$	155	0.357	2730	9.2×10^{-2}
SLDMS11-H_2	Cu	6.65	$5.0(2.0)\times10^{-4}$	180	0.380	2910	1.6×10^{-1}

In principle the hydrogen equation of state could be generated using the measured 300 K isotherm[10] and adding thermal pressure to it. However, this requires knowledge of Gruneisen parameters, heat capacities, and latent heats of fusion, which are not known accurately at these high pressures.

V. CELL CONSTANT

To derive electrical resistivities from the measured resistances the cell constant must be known. If the resistivity ρ of the sample is spatially uniform, the measured resistance R must be directly proportional to ρ, so that

$$R = C_1 \rho, \tag{1}$$

where C_1 is a geometry-dependent parameter called the cell constant.

To determine C_1, we performed steady-state, three-dimensional (3D) current-flow computer simulations of our sample-probe geometry. The assumption of steady-state current flow is justified by the fact that the measurement time is much longer than the magnetic flux diffusion time through the sample. The sample was simulated computationally by means of a finely meshed, 3D network of resistors, and the voltages of the nodes adjacent to the positive and negative electrodes were set equal to $+1$ and -1 V, respectively. By requiring that the net current flow into any node is zero (Kirchoff's law), a self-consistent solution for this network was found by an iterative method. The resistance is then simply $R = 2\ \mathrm{V}/I_{\mathrm{total}}$, where I_{total} is the total current flowing between the probes. The resistivity of the 3D cubic resistor network is determined by the grid spacing (the number of resistors) and the value of the individual resistors. We used a network of 400 Ω resistors with a 3D node separation of 25 μm to give a network resistivity of $\rho = 1\ \Omega$ cm. From this ρ and R the cell constant C_1 was found using Eq. (1) for the two-probe configuration.

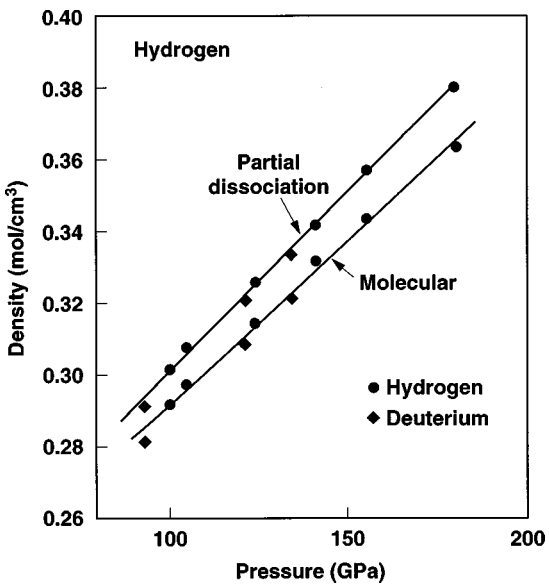

FIG. 6. Densities of hydrogen and deuterium calculated with model of Ross (Partial dissociation, Ref. 26) and model of Kerley (Molecular, Ref. 68) plotted versus pressure, P_f in Fig. 4.

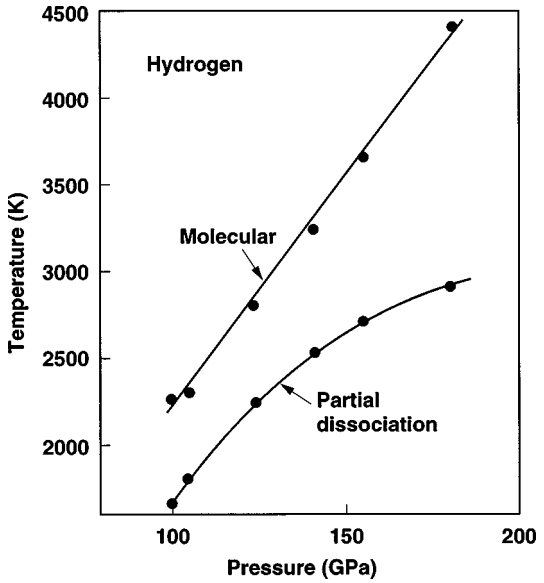

FIG. 7. Temperatures of hydrogen calculated with models of Ross (Partial dissociation) and Kerley (Molecular) plotted versus pressure, P_f in Fig. 4. At pressures above 130 GPa, Ross' calculated temperatures increase slower with pressure because energy is absorbed in molecular dissociation.

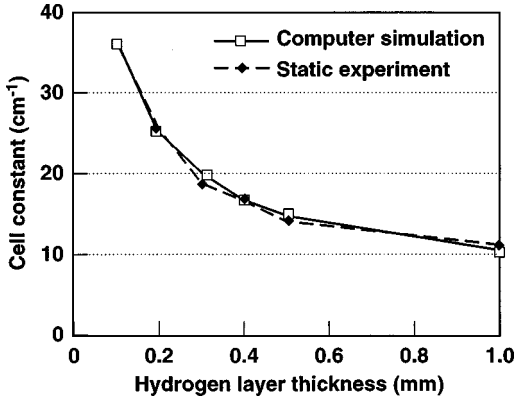

FIG. 8. Cell constants for two-probe configuration. Static calibration experiments were performed with an electrolytic solution for layer thicknesses of 0.2–1.0 mm. Computer simulations are described in text. For hydrogen layer thicknesses of ~0.05 mm in experiments, cell constants were calculated with computer simulation.

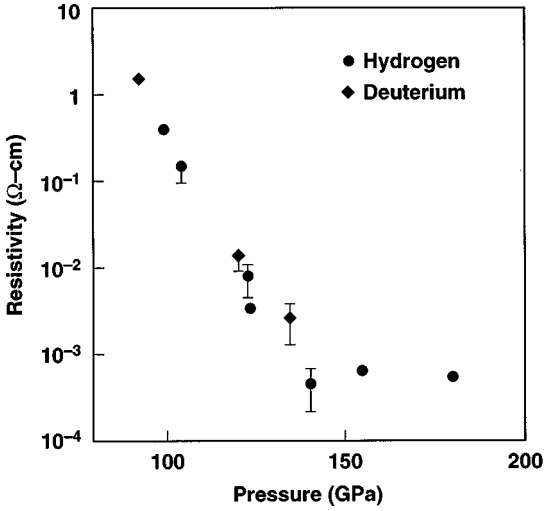

FIG. 9. Logarithm of electrical resistivity of H_2 and D_2 plotted versus pressure. Slope change at 140 GPa is transition from semiconducting to metallic fluid. H_2 and D_2 were used to reach different temperatures and densities.

For the four-probe geometry, in addition to the outer probes fixed at +1 and −1 V potential, there were two inner voltage probes between the two outer current probes. The voltages of these inner probes were not fixed, but were allowed to float. However, since we assume that the electrical conductivity of the metal probes is much higher than that of the sample, the voltages of the nodes adjacent to each inner probe must all be equal to each other. Since the impedance of the 50 Ω coaxial cables connected to the inner probes is much higher than the resistance of the sample between the inner probes, we assume that the inner probes draw negligible current. By noting the total voltage drop across the inner probes V_{inner} a second cell constant C_2 relates V_{inner} to the sample resistivity for the four-probe geometry:

$$V_{\text{inner}}/I_{\text{total}} = C_2\rho. \tag{2}$$

Thus, in the case of a four-probe experiment, we have two separate methods of determining the resistivity ρ, given by Eqs. (1) and (2). Using the inner probes and Eq. (2) is preferred. That is, since the inner probes draw little current, V_{inner} should be insensitive to contact resistances, and so measurements with the inner probes allow us to virtually eliminate contact resistance effects. If contact resistances were significant, then resistivity measurements using the voltage drop across the outer probes and Eq. (1) should give higher resistivities than those calculated using Eq. (2). Within the resolution both methods give the same values. Thus, contact resistance is negligible.

For these calculations the electrode surfaces were assumed to be flush with the interface between hydrogen and sapphire. In actuality the electrodes move into the hydrogen a few 10 μm in ~50 ns because the shock impedances of steel and sapphire are not identical. However, perturbation of the current flow by this motion is small because the hydrogen layer is thin (~50 μm).

Figure 8 is a plot of C_1 as a function of sample thickness for the two-probe geometry. The calculated curve was determined using the method outlined above with a 3D resistor network simulating an 8 mm×8 mm area around the electrodes; thicknesses were 1.0 mm or less. Since current flow is concentrated between the electrodes, we find that the results are insensitive to the use of larger volumes. Also shown in Fig. 8 are the cell constants determined by electrical measurements in a mock experimental static cell with an electrolytic solution to represent the sample. As seen in Fig. 8, agreement between the two methods of determining C_1 is excellent for layer thicknesses at which both calculations and experiments were performed (0.2–1.0 mm). Because of this good agreement, the cell constant was simply calculated for the ~50 μm layer thicknesses in the shock experiments.

The results for thicknesses below 200 μm were fit to the relation $C = Ax^{-1}$, where A is a constant and x is the thickness of the sample layer in cm. The following cell constants were obtained: (a) Two-probe geometry (C_1) with two probes 1.0 mm in diameter with centers separated by 3.5 mm: $A = 0.390$. (b) Four-probe geometry (C_1) with four probes 0.75 mm in diameter with centers of adjacent probes separated by 1.5 mm using only the two outer probes: $A = 1.144$. (c) Four-probe geometry (C_2) with four probes 0.75 mm in diameter with centers of adjacent probes separated by 1.5 mm: $A = 0.312$. The cell constant for a particular experiment was obtained by calculating the final hydrogen thickness and applying the appropriate relation above. The electrical resistivities determined from the measured resistances and appropriate cell constants are listed in Table I.

VI. SEMICONDUCTING FLUID HYDROGEN

The purpose of this analysis is to show that the mobility gap decreases relatively rapidly with density as the metallic state is approached. The experimental data are plotted as $\log_{10}(\rho)$ versus pressure in Fig. 9. The electrical resistivities decrease from about 1 Ω cm at 93 GPa to 5×10^{-4} Ω cm at 140 GPa and are constant within the error bars between 140 and 180 GPa. When plotted versus pressure, $\log_{10}(\rho)$ follows the same curve for both hydrogen and deuterium because density and temperature increase monotonically with pressure for both isotopes.[15] The change in slope at 140 GPa is indicative of the transition to the metallic state. We analyzed

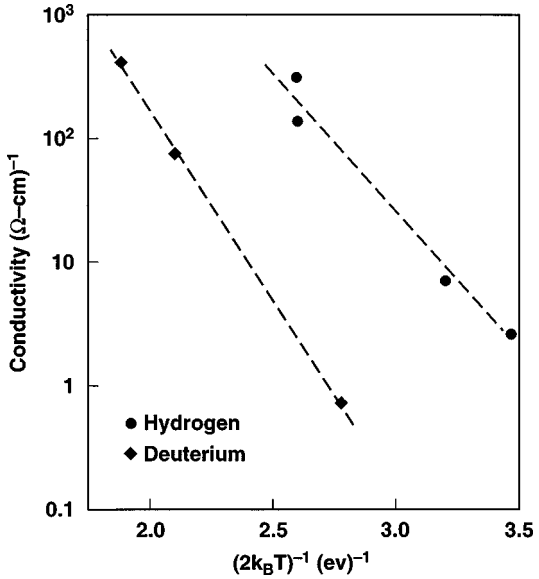

FIG. 10. Logarithm of electrical conductivities of H_2 and D_2 plotted versus $(2k_BT)^{-1}$. The dashed lines are guides to the eye.

results in the range 93–120 GPa, a semiconducting regime, by fitting the data to[21]

$$\sigma = \sigma_0 \exp[-E_g(D)/2k_BT], \tag{3}$$

where σ is electrical conductivity, σ_0 depends on density D, $E_g(D)$ is the density-dependent mobility gap in the electronic density of states of the fluid, k_B is Boltzmann's constant, and T is temperature.

Six data points with error bars of 20 to 50% were fit to Eq. (3). These error bars are sufficient because the conductivity varies almost four orders of magnitude. The error bars were caused primarily by signal dispersion in the low thermal-conductance steel coaxial cables used in most of the experiments. Signal dispersion was much less for Cu coaxial cables. For these six points density varied from 0.291 to 0.326 mol/cm^3 and temperature was in the range 1700 to 2800 K. The data are plotted as $\log_{10}(\sigma)$ versus $(2k_BT)^{-1}$ in Fig. 10. In this plot the data split systematically into results for hydrogen and for deuterium. The reason is that at a given temperature, hydrogen and deuterium are at different densities, which means different energy gaps. (This difference in conductivity is not caused by an isotope effect). Because of the relatively few data points and their error bars, the fitting function was chosen such that σ_0 is a constant in this range of density, $E_g(D)$ is assumed to vary linearly with density, and temperature dependences in σ_0 and $E_g(D)$ are neglected. The measured conductivities and the densities and temperatures calculated with Ross' model were least-squares fit to Eq. (3). The conductivity values calculated from this fit differ from the measured values by the magnitude of the error bars. The results of this least-squares fit to Eq. (3) are

$$E_g(D) = 1.22 - (62.6)(D - 0.30), \tag{4}$$

where $E_g(D)$ is in eV, D is in mol/cm^3 (0.29–0.32), and $\sigma_0 = 90\,(\Omega\ \mathrm{cm})^{-1}$. Because of the experimental uncertainties, the results of the least-squares fit are sensitive to the initial parameters chosen in the fitting procedure. Examination of several fits shows that the density at which $E_g(D) \rightarrow 0$ varies by 2% and the slope of $E_g(D)$ varies by 20%. These uncertainties are adequate for describing the NMM transition. Similar fitting results were obtained using Kerley's calculated densities and temperatures:[15] $E_g(D) = 0.905 - (67.7)(D - 0.30)$ and $\sigma_0 = 140\,(\Omega\ \mathrm{cm})^{-1}$. A value of $\sigma_0 = 200$–$300\,(\Omega\ \mathrm{cm})^{-1}$ is typical of liquid semiconductors.[71] The fact that the fits give σ_0 within a factor of 2–3 of the typical result shows that this result is reasonable. Chacham and Louie[7] showed theoretically that the electronic bandgap of the hcp solid at $T = 0$ K decreases linearly with density as metallization is approached. Their calculated rate of bandgap closure is 40 eV/(mol/cm^3), which is comparable to our value of ~60 eV/(mol/cm^3).

The $E_g(D)$ derived from this fitting procedure and k_BT are equal at a density of 0.32 mol/cm^3 and a temperature of ~2600 K (0.22 eV). In this region the energy gap is smeared out thermally, activation of electron carriers is complete, disorder is saturated in the fluid, and conductivity is expected to be weakly sensitive to further increases in pressure and temperature, provided the nature of the fluid does not change significantly. At 0.32 mol/cm^3 the calculated pressure is 120 GPa, which is close to the 140 GPa pressure at which the slope changes in the electrical resistivity (Fig. 6 indicates that a 20 GPa pressure difference corresponds to a 6% density shift). The initial 10% increase in density from 0.29–0.32 mol/cm^3 causes the bandgap to decrease from 1.8 eV to ~0.25 eV, where it is filled in by fluid disorder and thermal smearing. Thus, fluid hydrogen becomes metallic at about 140 GPa and ~2600 K via a continuous transition from a semiconducting to metallic fluid.

Because conductivities are thermally activated in the semiconducting regime (Fig. 10), it is probable that electronic states at the Fermi level of this disordered material are localized, as in alkali-metal fluids undergoing the NMM transition.[72] Because densities were not measured, it is not possible to know experimentally if a density discontinuity occurs at metallization. Nevertheless, it is our opinion that because of the high densities and temperatures, a density discontinuity does not occur at metallization.

VII. METALLIC FLUID HYDROGEN

The metallization process in dense fluid hydrogen is quite complex and not yet understood in detail.[73] However, the following is a simple preliminary discussion whose main goals are to show that our measured value of metallic conductivity is reasonable and to develop a simple picture of the nature of this metallic fluid.

A. Metallization process

Since these experiments are at finite temperatures in the disordered fluid, the density of electron states (DOS) around the Fermi level is not zero, as for a crystalline semiconductor at $T = 0$ K. Thermal smearing and disorder cause a small, nonzero DOS near the Fermi level in semiconducting fluid hydrogen.[74] Increasing pressure reduces the 15 eV bandgap and thermal disorder fills it in. When pressure and temperature are such that $E_g/k_B = T \sim 2600$ K, the depression in the bandgap is filled in, a metallic density of states is achieved, and the electronic system has a Fermi surface characteristic

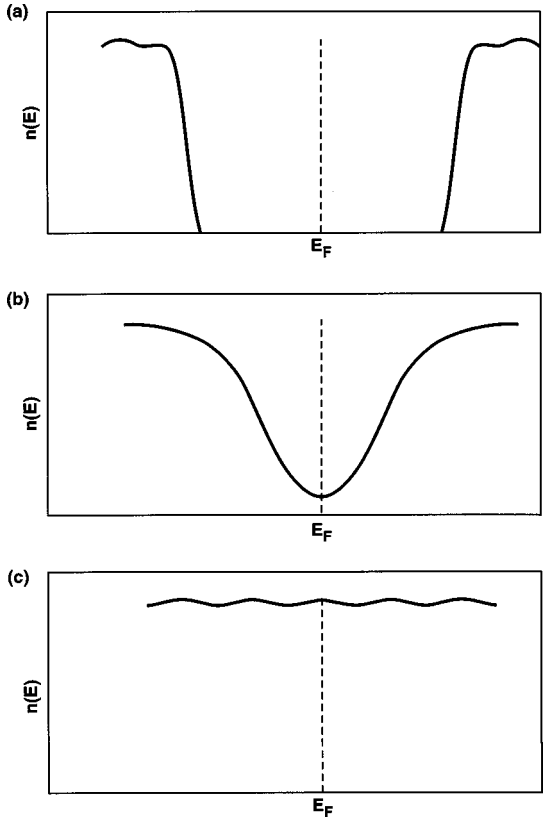

FIG. 11. Schematic electron densities of states near Fermi energy E_F in fluid hydrogen: (a) insulator at low pressures ($P<50$ GPa); (b) semiconductor at intermediate pressures ($50<P<140$ GPa) (Ref. 74); (c) metal at high pressures ($P>140$ GPa). Because conductivity is thermally activated in semiconducting fluid (b), states around E_F are probably localized and electron carriers are excited across mobility gap.

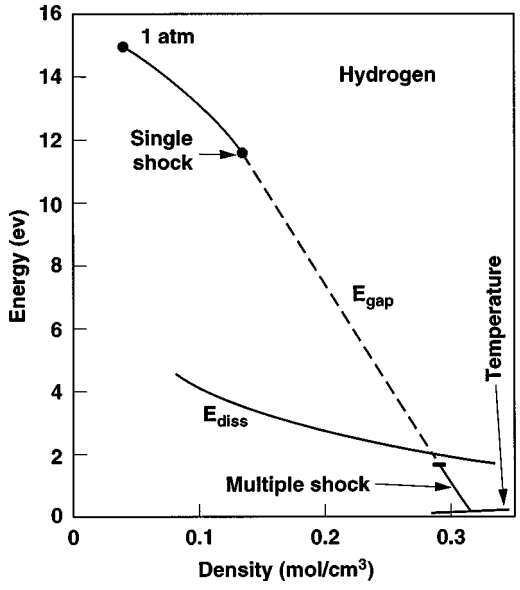

FIG. 12. Characteristic energies plotted versus density: electronic mobility gap $E_{\rm gap}$ [Ref. 21 and Eq. (4)], molecular dissociation energy $E_{\rm diss}$ extrapolated from Ross' model (Ref. 26), and calculated temperatures k_BT achieved in these experiments.

of a metal. This process is similar to those in conventional liquid semiconductors[75] and is illustrated in Fig. 11.

Characteristic energies are plotted versus density in Fig. 12. E_g produced by single-shock compression[21] is the point at 0.13 mol/cm^3. The linear dependence of E_g near 0.3 mol/cm^3 was determined in the present multiple-shock experiments [Eq. (4)]. These two determinations are interpolated linearly by the dashed line. The molecular dissociation energy $E_{\rm diss}$ was extrapolated from Ross' model.[26] The calculated temperatures in these conductivity experiments are also shown plotted as k_BT. Figure 12 shows that the temperatures are relatively low compared to E_g and $E_{\rm diss}$ and that these conductivity experiments are sensitive primarily to electronic excitation, with a relatively small amount of molecular dissociation. This is consistent with the suggestion that conduction in dense hydrogen is caused by electrons delocalized from H_2 molecules, which causes H_2^+ ions.[36] The free H_2^+ ion is quite stable, having a dissociation energy of 2.8 eV,[76] and thus it is reasonable to expect them to exist at these conditions. At metallization it is estimated[26,69,70] that about 10 at. % of the fluid is H monomers, assuming only H_2 and H need be considered.

B. Similarity of H_2 to Cs, Rb, and I_2

Hensel and Edwards have shown that fluid Cs and Rb at 2000 K are semiconducting fluids and that pressures of only $\sim$10 MPa are required to produce the minimum conductivity of a metal. The values of conductivities of metallic fluid Cs and Rb are essentially identical to those of fluid metallic hydrogen.[77] I_2 is a molecular system which undergoes the NMM transition by bandgap closure or thermal smearing at much lower pressures in the fluid than in the solid. Solid I_2 at 300 K becomes metallic at 16 GPa.[78] Fluid I_2 becomes metallic at only 3 GPa at 1000 K.[79] The pressure dependences of the resistivities of H_2 and I_2 are quite similar near metallization.[80]

C. Nature of the fluid

H_2 and H probably form a mutual solution. As shown in Fig. 13 the hydrogen atom and the spherically averaged molecule have essentially the same Bohr radius, based on calculations of Barbee.[81] The free hydrogen molecule is essentially spherical because the anisotropy in its charge distribution is only about 6%.[82] Because of their similar sizes and shapes and because the temperature of the fluid is $\sim$3000 K, molecules and atoms form a mixture and the measured electronic energy gap is that of the mixture. Based on similar energy gaps or ionization energies at low pressures, 15 eV for solid H_2 (Ref. 16) and 13.6 eV for the free atom, the energy gap of the mixture might not be very sensitive to the relative concentrations of molecules and atoms.

Tight-binding molecular dynamics calculations of Lenosky *et al.*[74] also show that fluid metallic hydrogen at 3000 K is essentially ''molecular.'' These simulations show a peak in the proton-proton pair distribution function at a distance corresponding to the separation between protons in the molecule. A low dissociation fraction of H_2 was estimated at $r_s=1.54$ (0.37 mol/cm^3) and 3000 K, which is in the metallic range. The strong tendency to have paired protons at high pressures has been noted by other authors as well.[5,7,26,83–86] At lower densities of 0.17 mol/cm^3 at 3000 K, this disordered semiconducting fluid is composed of a mixture of molecules and a few percent of atoms. A depression exists in the

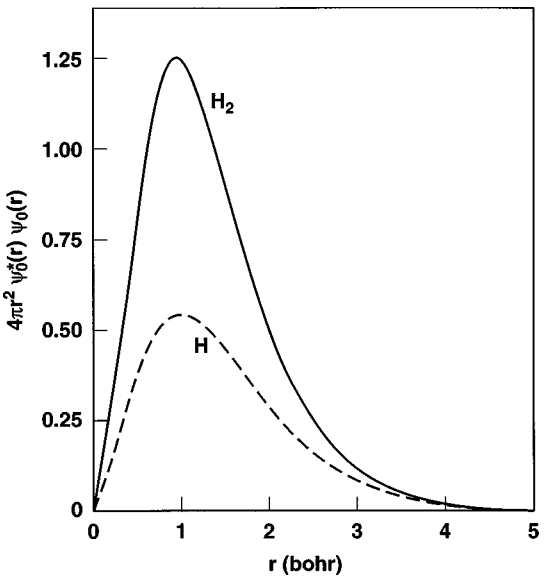

FIG. 13. Radial charge densities of ground-state wave functions of free H and spherically averaged free H_2 (Ref. 81). For H, r is measured from the nucleus; for H_2, r is measured from midpoint of molecular bond. Integrals under these curves are 1 and 2 for H and H_2, respectively.

DOS around the Fermi level. About half of the relatively few states at the Fermi level come from diatomic molecules and half from atoms, both of which occupy a common energy band.[74]

These MD simulations also show that ''molecules'' are short-lived (10^{-14}–10^{-13} sec). A proton pair exists for a few molecular vibrational periods and then on subsequent collision breakups into atoms, which combine with other atoms to form new dimers or remain unpaired as atoms, and so forth. Because of the short lifetimes, a better term to describe such an object is ''transient pair.'' It is also reasonable to assume that a particular electron might bind two protons into one H_2^+ transient pair and then be the conduction electron in its next transient pair. Several species, such as H_2^+, H_2, H^+, H, H_3^+,[87] and possibly higher order H clusters might be present. Presumably their compositions are constant if in fact such particles are well-defined at high densities and temperatures and if compositional averages are taken over a sufficiently long time interval, say 10^{-12} sec, which is shorter than the time resolution of our experiments, $\sim 10^{-9}$ sec. These MD simulations also show that kinetic, vibrational, and rotational energies of the transient pairs are comparable and dissociation commences at conditions near those for the onset of metallization. A fluid in which protons in transient pairs and monomers are continually exchanging on a timescale of $\sim 10^{-14}$ sec and in which characteristic times for collisions, vibrations, and rotations are comparable describes a new state of condensed matter.

In this tight-binding picture conduction electrons have a very short mean free path, namely, the distance between adjacent particles supplying conduction electrons. A conducting electron exchanges with its neighbor when electronic overlap is sufficiently large to allow an electron to hop to its nearest neighbor to produce a net current flow. This is a strong-scattering system and describes a state characteristic of the minimum conductivity of a metal. A similar model of electrons percolating in a non-ideal dense plasma has recently been developed.[88]

It is unlikely that the conductivity is caused simply by dissociated H atoms which form a distinct impurity band in insulating H_2. The MD calculations show that H_2 and H occupy a common band at the Fermi level.[74] In a degenerate solid semiconducting alloy, such as Si(P)[69,89] a distinct P band does form in the band gap of the Si host. Si has a very large dielectric constant, which reduces Coulomb repulsion and allows P atoms to interact at very large distances.[90] Si is a four-coordinated covalent semiconductor and P is a semimetal. The electronic structures of Si and P are very different from one another. H_2 and H have very similar electronic structures (Fig. 13). Because of the thermal disorder in fluid H_2 at $\sim$2000 K and disorder caused by rapid exchange of protons every $\sim 10^{-14}$ sec, we do not expect fluid H_2 to have a large macroscopic polarizibility and dielectric constant, except at metallization, and H monomers probably do not interact at long range. Nevertheless, the onset of metallization occurs near the onset of dissociation and its role in the NMM transition needs to be determined.

D. Fermi energy

We estimate the Fermi energy E_F in the free-electron model because of the high temperatures, the nearly spherical charge distributions (Fig. 13), and the energy band structure of solid molecular hydrogen becomes free-electron-like at high densities.[7,83] From Eq. (4) the electronic activation energy vanishes at $D_m = 0.32\,\mathrm{mol/cm^3}$. Because $E_g(D)$ decreases rapidly with density, this density of metallization is weakly sensitive to whether D_m is taken where $E_g = 0$ or $E_g = k_B T$. Because of the relatively low temperatures (Fig. 12), hydrogen is mostly molecular. Since the conductivities of fluid Cs and Rb are the same as that of hydrogen at metallization,[77] it is reasonable to assume that one conduction electron is supplied by each H_2, just as one conduction electron is supplied by each alkali atom. The fact that some hydrogen monomers formed by dissociation are mixed with hydrogen dimers and that some alkali dimers are mixed with alkali monomers is neglected for this simple estimate. Thus, total conduction electron density at metallization is $D_m \sim 1.9\times 10^{23}/\mathrm{cm^3}$, which corresponds to a free-electron Fermi energy of $E_F = 12$ eV, as for Al. Since the calculated temperature at metallization is $T = 0.22$ eV, $T/T_F \sim 0.02$ and this system is highly degenerate. If all electrons are itinerant, then E_F would be a factor $2^{2/3} = 1.6$ larger.

E. Mott transition

The fluid systems at $\sim$2000 K of Cs, Rb, and hydrogen all metallize with the same electrical conductivity of 2000 $(\Omega\,\mathrm{cm})^{-1}$. These fluids also obey the same condition of metallization, namely, the scaled density $= D_m^{1/3} a^* = C$, where D_m is the number density of conduction electrons and a^* is the effective Bohr radius. This scaled density is simply the ratio of two length scales, namely, the ratio of the size of the free particle a^* to the average distance between particles at metallization $D_m^{-1/3}$. This condition is essentially the same for both a Mott-Hubbard transition and for Anderson local-

ization. Because of the finite temperatures the measured saturation conductivity is probably caused by a Mott transition; Anderson localization occurs only at $T=0$ K.[91] This transition to the metallic fluid occurs at the same value of $D_m^{1/3}a^*=0.38$ for all three fluids, assuming hydrogen is monomeric.[77] Because of considerations above, we now believe that the majority constituent of metallic hydrogen is effectively a molecule. Since the Bohr radii of H and H_2 are essentially equal (Fig. 13), the scaled electron densities for monatomic and diatomic hydrogen differ simply by the factor $2^{1/3}$. Thus, for pure H_2, metallization occurs at $D_m^{1/3}a^*=0.30$. The value of $D_m^{1/3}a^*$ is not very sensitive to whether hydrogen is diatomic or monatomic and the value at metallization for both is close to Mott's preferred value of $D_m^{1/3}a^*=0.25$.[92] Although $D_m^{1/3}a^*$ is simply the ratio of two length scales, at metallization it is quite likely that many-body correlations are important. Thus, fluid hydrogen undergoes a Mott transition when the electronic charge densities on neighboring molecules are compressed together to produce sufficient overlap that a conduction electron is delocalized.

F. Comparison with available theories

We now compare the measured metallic conductivity with existing simple theories to see if our measured value is reasonable. The Drude conductivity, σ, is given by

$$\sigma=ne^2\tau/m, \tag{5}$$

where n is the number of electrons per unit volume, e and m are the charge and mass of the electron, respectively, and τ is the relaxation time for electron scattering. Since our measured metallic conductivity is the minimum conductivity of a metal, $\sigma_{\min}$, the relaxation time is given by the Ioffe-Regel[93] condition $\tau=d/v_F$, where d is the electron mean free path, equal to the average nearest-neighbor distance, and v_F is the Fermi velocity. In this case Eq. (5) reduces to[94]

$$\sigma_{\min}=e^2/(3\hbar d), \tag{6}$$

where $\hbar$ is $h/2\pi$, h is Planck's constant, and $d=D_m^{-1/3}$. Thus, $\sigma_{\min}=4000\,(\Omega\,\mathrm{cm})^{-1}$, which is in good agreement with the measured value of 2000 $(\Omega\,\mathrm{cm})^{-1}$.

If n is taken as $n(E_F)$, the number density of conduction electrons per unit volume at the Fermi energy E_F, then n must be reduced by $(1.5/E_F)$ (Ref. 95) and

$$\sigma=(1.5/E_F)\sigma_{\min}. \tag{7}$$

Then $\sigma=500\,(\Omega\,\mathrm{cm})^{-1}$, which is within a factor of 4 of the measured value.

The Ziman model[96] typically yields calculated values of resistivity in good agreement with experimental values for liquid metals. However, metallic hydrogen differs from typical liquid metals in that it retains a strong proton-pairing character, other species are probably present such as monomers and perhaps higher order clusters, protons comprising these dimers exchange on a time scale of $\sim10^{-14}$ sec, and conducting electrons are strongly scattered. Because of the high densities and temperatures, collisional, vibrational, and rotational times are comparable. Thus, standard theories for the electrical resistivity of liquid metals do not apply directly to this situation. For example, the Ziman model is a weak-scattering model. However, for comparison Louis and Ashcroft applied the Ziman formalism to liquid diatomic hydrogen with a free-electron DOS. They calculated a resistivity of 50–100 $\mu\Omega\,\mathrm{cm}$,[73] a factor of 5–10 lower than the experimental value. The factor of 5–10 required to match the experimental value can probably be accounted for by strong scattering, caused largely by the absence of core electrons.

The electrical conductivity of fluid metallic hydrogen has been calculated using tight-binding molecular dynamics. At 140 GPa and temperatures in the range 1500 to 3000 K, the calculated resistivities are 500 to 250 $\mu\Omega\,\mathrm{cm}$, respectively,[74,97] which is within a factor of 2 or less of the measured value. Since in this model the theoretical energies of the ground and antibonding electronic states of H_2 have a global error of order 0.01 Ry/atom (1600 K) or more, which is comparable to the temperatures in these experiments, the calculated conductivities give good qualitative trends but the calculated values are uncertain.

G. Optical skin depth

The optical depth is obtained from the complex part of the refractive index and is determined by the electrical conductivity and the frequency of the optical radiation.[98] We assume for the purpose of making a simple estimate, that conductivity is independent of frequency ω. The optical depth was calculated at the peak of the black-body spectrum at 3000 K, a wavelength of 1 μm, or an angular frequency $\omega=1.9\times10^{15}$/sec. The relaxation time, $\tau=D_m^{-1/3}/v_F$, is 8.5×10^{-17} sec. Thus, $\omega\tau=0.16$, which is in the low-frequency limit. For a conductivity of 2000 $(\Omega\,\mathrm{cm})^{-1}$, the optical depth is 640 A.

H. Phase-dependent metallization pressure

A key question is why is the metallization pressure of 140 GPa in the warm fluid, so different from recent predictions, ~300 GPa in the cold solid. Several phenomena are probably responsible. Phase transition pressures are temperature-dependent in general,[99] and the NMM transition pressure decreases with temperature.[43] The features which inhibit metallization of hydrogen in the ordered solid are probably crystalline and orientational phase transitions,[44,45] which do not exist in the disordered melt. Also, the electronic energy gap is reduced when the protons of a diatomic molecule extend their separation in thermally excited molecular states.[73] High temperatures in the fluid also cause molecules to approach closer to one another than they would at the same density at 0 K.[69] Thus, a molecule in the fluid samples a range of local structures, the energy gap is structure dependent, and structures with lower gaps than that of the solid are probably sampled in the fluid. Many-body effects also are important in the regime where metallization occurs.[73] In short, our observed metallization pressure is for a different phase and temperature than assumed by previous theoretical predictions.

VIII. COMPARISON BETWEEN EXPERIMENTS AT SHOCK AND STATIC PRESSURES

Solid-solid transitions within the molecular phase are observed in diamond-anvil experiments near a triple point at

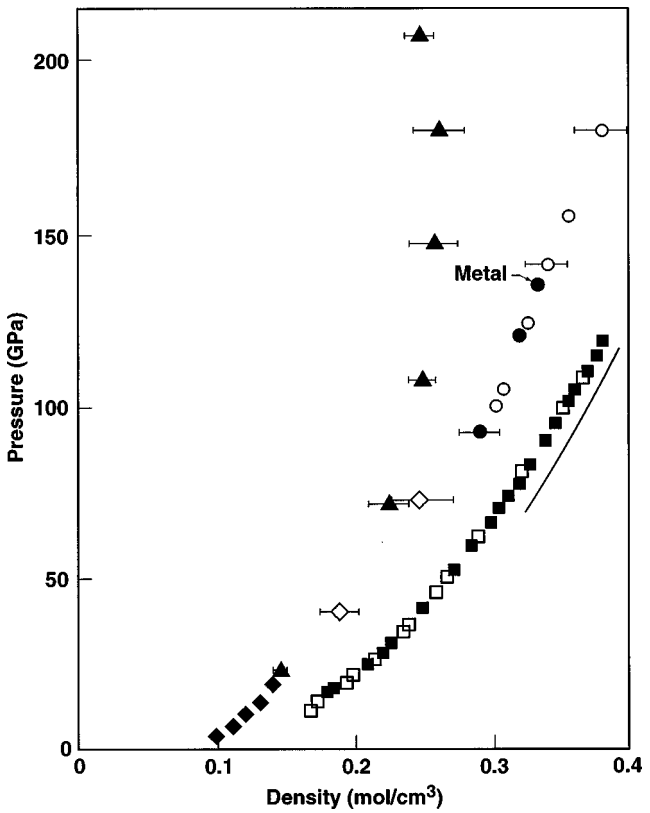

FIG. 14. Pressure-volume curves for (i) fluid states achieved in this work in H_2 (open circles) and D_2 (solid circles); (ii) solid states achieved in diamond anvil experiments at 300 K on H_2 (open squares) and D_2 (solid squares) (Ref. 10); theoretical 0-K isotherm (solid curve) calculated for H_2 hcp phase (Ref. 101); D_2 Hugoniot points obtained with gas gun under single shock (solid diamonds) and double shock (open diamonds) (Ref. 25); D_2 Hugoniot points obtained with laser (solid triangles) (Ref. 27).

150 GPa and 150 K.[41,100] This pressure is close to that at which metallization is observed in the fluid.

The crystal structure of solid hydrogen and deuterium has been determined by x-ray diffraction to be hcp at pressures up to 109 and 119 GPa, respectively, at room temperature.[10] The experimental P-V data for solid H_2 and D_2 lie on a common curve of pressure versus molar density, as shown in Fig. 14. Above 70 GPa these data for the solid are in good agreement with the 0-K isotherm of the hcp phase calculated by Barbee *et al.*[101] Also shown in Fig. 14 are the calculated states in the fluid achieved in these conductivity experiments (Table I). At a given density the pressure in the fluid is substantially higher than in the solid. The exact reason needs to be determined. However, one possible explanation is the fact that hydrogen, because it is so light, is the softest of all solids, in the sense that pressure increases relatively slowly with density at 0 K. On the other hand, fluid hydrogen at high pressures and temperatures has compressions[25] which are similar to those of other small molecular systems, such as nitrogen.[102] Thus, the difference between the 0-K isotherm of the solid and the fluid states in these experiments might be caused by the fact that solid hydrogen is so soft. On the other hand, if the densities in these conductivity experiments are 6% greater than in Table I as suggested by the difference between the observed and calculated pressure of the slope change in resistivity, then the relatively large difference between the static P-V data and the densities calculated in these experiments is reduced significantly.

The fact that metallization of hydrogen in the fluid occurs at ninefold compression of initial liquid density is in agreement with the theoretical prediction that solid molecular hydrogen should become metallic by band overlap in the $Pa3$ structure at nine times initial solid density.[83] The $Pa3$ structure mimics the high coordination and orientational averaging in a liquid. A similar comparison with theoretical results for the metallization volume of the orientationally disordered hcp phase is not as favorable, 1.9 cm^3/mol for the orientationally disordered solid versus 2.5 cm^3/mol for the orientationally ordered hcp solid.[7]

Generally, however, static and dynamic experiments and theory all indicate that the nature of molecular hydrogen changes at about 150 GPa and the nature of the change depends on temperature. Recent Hugoniot measurements in the range 23 to 200 GPa (Ref. 27) are also shown in Fig. 14, along with our previous Hugoniot data.[25] All the data in Fig. 14 are at ~100 GPa pressures and temperatures of ~1 eV or less. A common theory is needed to understand all these results.

ACKNOWLEDGMENTS

This work was performed under the auspices of the U.S. Department of Energy under Contract No. W-7405-ENG-48. We acknowledge N. W. Ashcroft for scientific discussions and encouragement. We thank M. Ross, T. W. Barbee, III, and A. A. Louis for discussions and calculational results. We acknowledge discussions with F. Hensel, P. P. Edwards, L. A. Collins, T. J. Lenosky, N. C. Holmes, D. A. Young, R. Chau, J. D. Johnson, R. Cheret, A. U. Hazi, C. Mailhiot, R. J. Hemley, H.-K. Mao, A. L. Ruoff, I. F. Silvera, F. Datchi, P. Loubeyre, D. J. Stevenson, W. B. Hubbard, J. R. Asay, T. J. Ahrens, R. Jeanloz, M. H. Manghnani, A. A. Abrikosov, B. Alder, R. B. Laughlin, D. Logan, V. E. Fortov, V. V. Yakushev, S. I. Anisimov, S. Pollaine, S. J. Rothman, M. D. Furnish, H. C. Vantine, R. Minich, E. A. Chandler, D. Herschbach, E. W. Burke, H. D. Shay, P. A. Dowben, P. F. McMillan, A. Bunker, E. Teller, S. B. Libby, N. Snyderman, J. C. Angus, M. Balooch, K. Kulander, D. C. Christian, and M. B. Brodsky. We acknowledge E. See, P. McCandless, J. Crawford, S. Weaver, K. Stickle, W. Brocious, R. Silva, and C. R. Henry for technical assistance. We thank R. Kays of Lockheed-Martin for loaning a storage dewar for liquid-H_2 coolant. This research was performed with support from the LLNL Directed Research and Development Program for which we thank J. F. Holzrichter, F. S. Dietrich, and E. A. Henry.

APPENDIX

1. Thermal equilibrium

Metallic fluid hydrogen is in thermal equilibrium. Using the average distance between the centers of two adjacent molecules, 1.7 A, ideal-gas thermal velocity, and a constant vibron frequency,[41] within the 3-ns time resolution there are ~10^5 intermolecular collisions with 4 times as many molecular vibrations.

2. Electrical equilibrium

The calculated flux diffusion time[103] for a layer 50-μm thick with an electrical conductivity of 2000 $(\Omega\,\mathrm{cm})^{-1}$ is <1 ns, which indicates that the electrical current reaches its equilibrium flow pattern in <1 ns.

3. Hydrodynamic instabilities and edge effects

Richtmyer-Meshkov[104,105] (RM) instabilities did not occur at the planar interfaces between sapphire and hydrogen because the surfaces of the strong sapphire crystals were optically flat and the time duration of the experiment too short ($\sim$100 ns) to allow interfacial instabilities to grow. The shock front induced by impact lies within a few 0.1° to the normal to the impact surface and the shock front has a small parabolic distortion of at most 20 μm.[47,49] When the first shock of $\sim$5 GPa enters the hydrogen, any possible low-density, gaseous surface ejecta are tamped by hydrogen compressed to twice its initial liquid density and this interface is maintained. The issue then is the stability of the interfaces between Al_2O_3 and hydrogen as the shock reverberates up to peak pressure. To insure that our interfaces were stable: (i) the sapphire anvils were optically flat, (ii) Al_2O_3 strength was maintained because the estimated temperature of the multiply shock-compressed Al_2O_3 adjacent to the hydrogen is $\sim$1000 K at 150 GPa, well below its estimated melting temperature, which probably exceeds 3000 K at 150 GPa based on melting temperatures of strong MgO,[106] (iii) the time duration of the experiment is short, $\sim$100 ns, to preclude growth of instabilities, and (iv) acceleration of the planar interfaces was zero except when relatively weak jumps in shock pressure occurred on shock reflections [Fig. 4(b)].

Four optical interference fringes spanned the 25-mm diameter of the sapphire disks, indicating a parabolic surface with a height difference of 2 μm between the center and the outer radius. This 50-mm-wavelength perturbation has negligible RM growth[107] of $\sim$0.1 μm in 100 ns. This disk also had a random surface roughness with an rms variation 300 A. If any short-wavelength perturbation should start to grow from this, it would be damped by the strength of Al_2O_3.

The thicknesses of Al, sapphire, and hydrogen were sufficiently small that the experiment was over before edge-release waves could affect the results. That is, the outer diameter of the impactor was 24 mm; the electrodes were located longitudinally 4.5 mm from the impact surface with a transverse separation of 5.3 mm between the extremities of the collinear arrangement of the four electrodes. Since current flow is concentrated between the electrodes, pressure release on the edges does not affect these measurements.

4. Radiative cooling

At 3000 K for 10^{-7} sec, 460 erg/cm^2 are radiated from hydrogen using the Stefan-Boltzmann law. The calculated heat capacity is $6.5\,R$/mol.[108] Since the optical depth at the peak of the 3000-K black body spectrum is 640 A, the heat capacity of the hydrogen radiating surface, about two optical depths, is 2400 erg/(cm^2 K). Thus, only $\sim$0.2 K out of 3000 K are lost by radiation.

5. Conductive cooling

Heat lost from hydrogen by thermal conduction into Al_2O_3 was calculated from the heat flow across an interface between two dissimilar materials.[109] Al_2O_3 temperature was taken as 1300 K, the estimated temperature produced by a single shock at 140 GPa.[66] Thermal conductivity of metallic hydrogen was calculated using the Wiedemann-Franz law. Values of thermal conductivity and thermal diffusivity of hydrogen were 0.15 W/cm K and 0.009 cm^2/sec, respectively. Values for alumina were 0.06 W/cm K and 0.015 cm^2/sec.[110] An interfacial layer about 0.5 μm thick is cooled about 200 K, negligible compared to the 50 μm total thickness at 3000 K.

6. Interfacial chemical reactions

High temperatures at the hydrogen-alumina interface raise the question of whether an interfacial chemical reaction might cause a thin metallic layer responsible for the measured resistance. This is not possible in the time available.

One possible reaction is the reduction of Al_2O_3 by hydrogen to cause a layer of free Al.[111] To estimate the resistivity of such a layer we assume an Al layer forms to the depth to which hydrogen diffuses and the diffusion coefficients of all species containing O and H are infinite. The diffusion coefficient of hydrogen was taken to be 10^{-2} cm^2/sec, or 10^3 larger than the typical self-diffusion coefficient of liquid metals, 10^{-5} cm^2/sec.[112] Thus, the diffusion length of hydrogen into alumina in $t=10^{-7}$ sec is 0.5 μm. A similar estimate is obtained from ion beam implantations of H_2^+ into alumina at 2×10^4 eV. To be certain that an Al-oxide layer was thick enough to stop all implanted H_2^+ ions, the Al oxide layer was chosen to be 0.2-μm thick[113] for an ion-beam energy 10^5 times larger than the temperature of hydrogen. So, we assume conservatively that a conducting interfacial layer is formed with a thickness of 0.5 μm. Based on Eq. (1), because the thickness would be 10^2 times smaller than for the bulk, the resistivity would be 10^{-2} times smaller than for the bulk. Thus, the resistivity of such a film would need to be $\sim$5 $\mu\Omega$ cm, comparable to crystalline Al at room temperature. It is not possible to obtain such a low resistivity in a disordered system at 3000 K.

7. Ionic conduction

Our measured conductivities are not caused by ions. Electrical conductivities[114] of ionic alkali-halide fluids are typically $\sim$1 $(\Omega\,\mathrm{cm})^{-1}$, while conductivities of pure metallic alkali fluids are typically a few 1000 $(\Omega\,\mathrm{cm})^{-1}$. We measured a metallic hydrogen conductivity of 2000 $(\Omega\,\mathrm{cm})^{-1}$, indicative of electronic charge carriers.

8. Shock-induced polarization

Shock-induced polarization in single-crystal Al_2O_3 is not responsible for our electrical signals. Shock pressures of about 10 GPa produce polarization voltage pulses in

plastics[115] and alkali halides[116] in high-capacitance geometries. In our experiments with Al_2O_3 (i) shock pressures are too large (>100 GPa) to induce such voltages, (ii) our detector geometry has an extremely tiny capacitance, (iii) our conductivity is measured differentially to eliminate any such voltages, and (iv) the electrical conductivity voltages of shock-compressed Al_2O_3 show no sign of shock-induced polarization.[54]

[1] E. Wigner and H. B. Huntington, J. Chem. Phys. **3**, 764 (1935).
[2] B. J. Alder and R. H. Christian, Phys. Rev. Lett. **4**, 450 (1960); B. J. Alder, in *Progress in Very High Pressure Research*, edited by F. P. Bundy, W. R. Hibbard, and H. M. Strong (Wiley, New York, 1961), pp. 152–164.
[3] H. K. Mao, P. M. Bell, and R. J. Hemley, Phys. Rev. Lett. **55**, 99 (1985).
[4] N. W. Ashcroft, Phys. Rev. B **41**, 10 963 (1990).
[5] M. Ross, F. H. Ree, and D. A. Young, J. Chem. Phys. **79**, 1487 (1983).
[6] A. Garcia, T. W. Barbee, M. L. Cohen, and I. F. Silvera, Europhys. Lett. **13**, 355 (1990).
[7] H. Chacham and S. G. Louie, Phys. Rev. Lett. **66**, 64 (1991); H. Chacham, X. Zhu, and S. G. Louie, Phys. Rev. B **46**, 6688 (1992).
[8] E. Kaxiras, J. Broughton, and R. J. Hemley, Phys. Rev. Lett. **67**, 1138 (1991).
[9] C. Narayana, H. Luo, J. Orloff, and A. L. Ruoff, Nature (London) **393**, 46 (1998).
[10] P. Loubeyre, R. LeToullec, D. Hausermann, M. Hanfland, R. J. Hemley, H. K. Mao, and L. W. Finger, Nature (London) **383**, 702 (1996).
[11] H. N. Chen, E. Sterer, and I. F. Silvera, Phys. Rev. Lett. **76**, 1663 (1996).
[12] R. J. Hemley, H. K. Mao, A. F. Goncharov, M. Hanfland, and V. Struzhkin, Phys. Rev. Lett. **76**, 1667 (1996).
[13] A. L. Ruoff, in *High Pressure Science and Technology*, edited by W. Trzeciakowski (World Scientific, Singapore, 1996), p. 511.
[14] W. J. Nellis, N. C. Holmes, M. Ross, S. T. Weir, and A. C. Mitchell, in *High Pressure Science and Technology*, edited by W. Trzeciakowski (World Scientific, Singapore, 1996), p. 521.
[15] S. T. Weir, A. C. Mitchell, and W. J. Nellis, Phys. Rev. Lett. **76**, 1860 (1996).
[16] K. Inoue, H. Kanzaki, and S. Suga, Solid State Commun. **30**, 627 (1979).
[17] V. Diatschenko, C. W. Chu, D. H. Liebenberg, D. A. Young, M. Ross, and R. L. Mills, Phys. Rev. B **32**, 381 (1985).
[18] F. Datchi and P. Loubeyre (private communication).
[19] M. Ross, H. C. Graboske, and W. J. Nellis, Philos. Trans. R. Soc. London, Ser. A **303**, 303 (1981).
[20] W. B. Hubbard, T. Guillot, J. I. Lunine, A. Burrows, D. Saumon, M. S. Marley, and R. S. Freedman, Phys. Plasmas **4**, 2011 (1997).
[21] W. J. Nellis, A. C. Mitchell, P. C. McCandless, D. J. Erskine, and S. T. Weir, Phys. Rev. Lett. **68**, 2937 (1992).
[22] R. S. Hawke, T. J. Burgess, D. E. Duerre, J. G. Huebel, R. N. Keeler, H. Klapper, and W. C. Wallace, Phys. Rev. Lett. **41**, 994 (1978).
[23] M. van Thiel, M. Ross, B. L. Hord, A. C. Mitchell, W. H. Gust, M. J. D'Addario, and R. N. Keeler, Phys. Rev. Lett. **31**, 979 (1973).
[24] R. D. Dick and G. I. Kerley, J. Chem. Phys. **73**, 5264 (1980).
[25] W. J. Nellis, A. C. Mitchell, M. van Thiel, G. J. Devine, R. J. Trainor, and N. Brown, J. Chem. Phys. **79**, 1480 (1983).
[26] N. C. Holmes, M. Ross, and W. J. Nellis, Phys. Rev. B **52**, 15 835 (1995).
[27] L. B. Da Silva, P. Celliers, G. W. Collins, K. S. Budil, N. C. Holmes, T. W. Barbee, III, B. A. Hammel, J. D. Kilkenny, R. J. Wallace, M. Ross, and R. Cauble, Phys. Rev. Lett. **78**, 483 (1997).
[28] G. W. Collins, L. B. Da Silva, P. Celliers, D. M. Gold, M. E. Foord, R. J. Wallace, A. Ng, S. V. Weber, K. S. Budil, and R. Cauble, Science **281**, 1178 (1998).
[29] W. J. Nellis, M. Ross, and N. C. Holmes, Science **269**, 1249 (1995).
[30] W. J. Nellis, S. T. Weir, and A. C. Mitchell, Science **273**, 936 (1996).
[31] W. J. Nellis, Chem.-Eur. J. **3**, 1921 (1997).
[32] W. J. Nellis, S. T. Weir, N. C. Holmes, M. Ross, and A. C. Mitchell, in *Properties of Earth and Planetary Materials at High Pressure and Temperature*, edited by M. H. Manghnani and T. Yagi (American Geophysical Union, Washington, 1998), pp. 357–364.
[33] W. J. Nellis, Plan. Space Sci. (to be published).
[34] J. D. Lindl, R. L. McCrory, and E. M. Campbell, Phys. Today **45** (9), 32 (1992).
[35] J. Lindl, Phys. Plasmas **2**, 3933 (1995).
[36] N. W. Ashcroft, Phys. Rev. Lett. **21**, 1748 (1968).
[37] C. F. Richardson and N. W. Ashcroft, Phys. Rev. Lett. **78**, 118 (1997).
[38] W. J. Nellis, Philos. Mag. (to be published).
[39] V. Bharadwaj, in *Proceedings of the 1995 Particle Accelerator Conference* (Institute of Electrical and Electronic Engineers, Piscataway, NJ, 1996), pp. 396–400.
[40] W. Kolos and L. Wolniewicz, J. Chem. Phys. **49**, 404 (1968).
[41] H. K. Mao and R. J. Hemley, Rev. Mod. Phys. **66**, 671 (1994).
[42] N. W. Ashcroft, J. Non-Cryst. Solids **156–158**, 621 (1993).
[43] E. Abrahams and G. Kotliar, Science **274**, 1853 (1996).
[44] N. W. Ashcroft, Phys. World **8**, 43 (1995).
[45] B. Edwards and N. W. Ashcroft, Nature (London) **388**, 652 (1997).
[46] A. C. Mitchell and W. J. Nellis, Rev. Sci. Instrum. **52**, 347 (1981).
[47] A. C. Mitchell and W. J. Nellis, J. Appl. Phys. **52**, 3363 (1981); N. C. Holmes, J. A. Moriarty, G. R. Gathers, and W. J. Nellis, *ibid.* **66**, 2962 (1989).
[48] D. Erskine, in *High-Pressure Science and Technology-1993*, edited by S. C. Schmidt, J. W. Shaner, G. A. Samara, and M. Ross (American Institute of Physics, New York, 1994), pp. 141–143.
[49] W. J. Nellis and A. C. Mitchell, J. Chem. Phys. **73**, 6137 (1980).
[50] A. C. Mitchell and W. J. Nellis, J. Chem. Phys. **76**, 6273 (1982).
[51] H. B. Radousky, W. J. Nellis, M. Ross, D. C. Hamilton, and A. C. Mitchell, Phys. Rev. Lett. **57**, 2419 (1986).
[52] D. C. Hamilton, W. J. Nellis, A. C. Mitchell, F. H. Ree, and M. van Thiel, J. Chem. Phys. **88**, 5042 (1988).
[53] W. J. Nellis, D. C. Hamilton, N. C. Holmes, H. B. Radousky, F.

H. Ree, A. C. Mitchell, and M. Nicol, Science **240**, 779 (1988).
[54] S. T. Weir, A. C. Mitchell, and W. J. Nellis, J. Appl. Phys. **80**, 1522 (1996).
[55] N. Funamori and R. Jeanloz, Science **278**, 1109 (1997).
[56] R. Chau, W. J. Nellis, A. C. Mitchell, and R. W. Minich (unpublished).
[57] N. C. Holmes, W. J. Nellis, W. B. Graham, and G. E. Walrafen, Phys. Rev. Lett. **55**, 2433 (1985).
[58] V. E. Fortov, A. S. Filimonov, S. V. Kvitov, D. N. Nikolaev, V. I. Postnov, V. Ya. Ternovoi, and A. V. Utkin, Bull. Am. Phys. Soc. **42**, 1494 (1997).
[59] K. M. Ogilvie and G. E. Duvall, J. Chem. Phys. **78**, 1077 (1983).
[60] C. S. Yoo, G. E. Duvall, J. Furrer, and R. Granholm, J. Phys. Chem. **93**, 3012 (1989).
[61] G. A. Lyzenga and T. J. Ahrens, in *Shock Waves in Condensed Matter-1981*, edited by W. J. Nellis, L. Seaman, R. A. Graham (American Institute of Physics, New York, 1982), pp. 231–235.
[62] D. P. Dandekar and M. Hankin, in *Shock Compression of Condensed Matter-1989*, edited by S. C. Schmidt, J. N. Johnson, and L. W. Davison (Elsevier, Amsterdam, 1990), pp. 97–100.
[63] R. Minich (private communication).
[64] R. A. Graham and W. P. Brooks, J. Phys. Chem. Solids **32**, 2311 (1971).
[65] T. Mashimo, in *Shock Waves in Materials Science*, edited by A. Sawaoka (Springer-Verlag, Tokyo, 1993), pp. 113–144, and references therein.
[66] T. J. Ahrens, W. H. Gust, and E. B. Royce, J. Appl. Phys. **39**, 4610 (1968).
[67] A. P. Jephcoat, R. J. Hemley, and H. K. Mao, Physica B **150**, 115 (1988).
[68] G. I. Kerley, in *Molecular-Based Study of Fluids*, edited by J. M. Haile and G. A. Mansoori (American Chemical Society, Washington, 1983), pp. 107–138.
[69] M. Ross, Phys. Rev. B **54**, R9589 (1996).
[70] M. Ross, Phys. Rev. B **58**, 669 (1998).
[71] N. F. Mott, Philos. Mag. **24**, 2 (1971).
[72] D. E. Logan, I. J. Bush, and P. A. Madden, Z. Phys. Chem. (Leipzig) **184**, 25 (1994).
[73] W. J. Nellis, A. A. Louis, and N. W. Ashcroft, Philos. Trans. R. Soc. London, Ser. A **356**, 119 (1998).
[74] T. J. Lenosky, J. D. Kress, L. A. Collins, and I. Kwon, Phys. Rev. B **55**, R11 907 (1997).
[75] N. F. Mott and E. A. Davis, *Electronic Processes in Non-Crystalline Materials* (Oxford, London, 1971).
[76] L. Pauling and E. B. Wilson, *Introduction to Quantum Mechanics* (McGraw-Hill, New York, 1935), p. 330.
[77] F. Hensel and P. Edwards, Phys. World **4**, 43 (1996).
[78] B. M. Riggleman and H. G. Drickamer, J. Chem. Phys. **38**, 2721 (1963).
[79] V. V. Brazhkin, S. V. Popova, R. N. Voloshin, and A. G. Umnov, High Press. Res. **6**, 363 (1992).
[80] R. J. Hemley and N. W. Ashcroft, Phys. Today **51** (8), 26 (1998).
[81] T. W. Barbee, III (private communication).
[82] I. F. Silvera, Rev. Mod. Phys. **52**, 393 (1980).
[83] C. Friedli and N. W. Ashcroft, Phys. Rev. B **16**, 662 (1977).
[84] A. Ferraz, N. H. March, and F. Flores, J. Phys. Chem. Solids **45**, 627 (1984).
[85] S. I. Anisimov and Yu. V. Petrov, JETP Lett. **65**, 412 (1997).
[86] A. Bunker, S. Nagel, R. Redmer, and G. Ropke, Phys. Rev. B **56**, 3094 (1997).
[87] W. Meyer, P. Botschwina, and P. Burton, J. Chem. Phys. **84**, 891 (1986).
[88] A. A. Likalter, JETP **86**, 598 (1998).
[89] M. Besson, Phys. Rev. Lett. **78**, 5026 (1997).
[90] N. W. Ashcroft and N. D. Mermin, *Solid State Physics* (Holt, Rinehart, and Winston, New York, 1976), p. 579.
[91] P. W. Anderson, Phys. Rev. **109**, 1492 (1958).
[92] N. F. Mott and E. A. Davis, *Electronic Processes in Non-Crystalline Materials* (Oxford, London, 1971), p. 133.
[93] A. F. Ioffe and A. R. Regal, Prog. Semicond. **4**, 237 (1960).
[94] N. F. Mott and E. A. Davis, *Electronic Processes in Non-Crystalline Materials* (Oxford, London, 1971), p. 81.
[95] N. W. Ashcroft and N. D. Mermin, *Solid State Physics* (Holt, Rinehart, and Winston, New York, 1976), p. 44.
[96] J. M. Ziman, Philos. Mag. **6**, 1013 (1961).
[97] J. Kress, L. Collins, T. Lenosky, I. Kwon, and N. Troullier (unpublished).
[98] R. P. Feynman, R. B. Leighton, and M. Sands, *The Feynman Lectures on Physics* (Addison-Wesly, Reading, Mass., 1964), Vol. II, p. 32–10.
[99] D. A. Young, *Phase Diagrams of the Elements* (University of California Press, Berkeley, 1991).
[100] L. Cui, N. H. Chen, S. J. Jeon, and I. F. Silvera, Phys. Rev. Lett. **72**, 3048 (1994).
[101] T. W. Barbee, III, A. Garcia, M. L. Cohen, and J. L. Martins, Phys. Rev. Lett. **62**, 1150 (1989).
[102] W. J. Nellis, H. B. Radousky, D. C. Hamilton, A. C. Mitchell, N. C. Holmes, K. B. Christianson, and M. van Thiel, J. Chem. Phys. **94**, 2244 (1991).
[103] J. D. Jackson, *Classical Electrodynamics* (Wiley, New York, 1962), p. 313.
[104] R. D. Richtmyer, Commun. Pure Appl. Math. **13**, 297 (1960).
[105] E. E. Meshkov, Izv. Akad. Nauk SSSR, Mekh. Zhidk. Gaza **5**, 151 (1969).
[106] R. Boehler, M. Ross, and D. B. Boercker, Phys. Rev. Lett. **78**, 4589 (1997).
[107] K. O. Mikaelian, Phys. Rev. A **31**, 410 (1985).
[108] M. Ross (private communication).
[109] H. S. Carslaw and J. C. Jaeger, *Conduction of Heat in Solids* (Clarendon, Oxford, 1959), p. 88.
[110] *Thermophysical Properties of High Temperature Solid Materials, Volume 4: Oxides and Their Solutions and Mixtures*, edited by Y. S. Touloukian (MacMillan, New York, 1967), pp. 11–20.
[111] A. L. Ruoff (private communication).
[112] T. Iida and R. I. L. Guthrie, *The Physical Properties of Liquid Metals* (Clarendon, Oxford, 1988), p. 199.
[113] N. Imanishi, T. Fukumura, S. Miyamoto, and M. Iwasaki, J. Appl. Phys. **61**, 5485 (1987).
[114] W. W. Warren, Jr., in *The Metallic and Nonmetallic States of Matter*, edited by P. P. Edwards and C. N. R. Rao (Taylor and Francis, London, 1985), p. 142.
[115] G. E. Hauver, J. Appl. Phys. **36**, 2113 (1965).
[116] R. K. Linde, W. J. Murri, and D. G. Doran, J. Appl. Phys. **37**, 2527 (1966).